Perovskite heterojunction based on CH3NH3PbBr3 single crystal for high-sensitive self-powered photodetector

Min Cao, Jiyu Tian, Zhi Cai, Lan Peng, Lei Yang, and Dacheng Wei

Articles you may be interested in

High performance ultraviolet photodetectors based on ZnO nanoflakes/PVK heterojunction
Appl. Phys. Lett. **109**, 073103 (2016); 10.1063/1.4961114

Self-powered and broadband photodetectors based on graphene/ZnO/silicon triple junctions
Appl. Phys. Lett. **109**, 053501 (2016); 10.1063/1.4960357

Tunable bandgap in hybrid perovskite CH3NH3Pb(Br3−yXy) single crystals and photodetector applications
AIP Advances **6**, 045115 (2016); 10.1063/1.4948312

High efficiency sequentially vapor grown n-i-p CH3NH3PbI3 perovskite solar cells with undoped P3HT as p-type heterojunction layer
APL Mater. **3**, 016105 (2015); 10.1063/1.4905932

Self-powered solid-state photodetector based on TiO2 nanorod/spiro-MeOTAD heterojunction
Appl. Phys. Lett. **103**, 261109 (2013); 10.1063/1.4858390

Perovskite heterojunction based on CH$_3$NH$_3$PbBr$_3$ single crystal for high-sensitive self-powered photodetector

Min Cao,[a)] Jiyu Tian,[a)] Zhi Cai, Lan Peng, Lei Yang, and Dacheng Wei[b)]

Department of Macromolecular Science, Fudan University, Shanghai 200433, China

Perovskite single crystals exhibit extraordinary optoelectronic performances due to their advantages such as low trap-state densities, long carrier diffusion, and large absorption coefficient, and thus, photodetectors based on perovskite single crystals have attracted much research interest. Unlike the reported one-component single-crystal perovskite photodetectors, here, we have developed a facile two-step approach to fabricate a core-shell heterojunction based on the CH$_3$NH$_3$PbBr$_3$ single crystal. A photodetector made of the as-prepared perovskite heterojunction renders the feature of self-power attributed to a built-in electric field in the junction and exhibits a wavelength-dependent responsivity with a peak responsivity up to 11.5 mA W^{-1} under 450 nm irradiation at zero bias, which is one order of magnitude higher than the CH$_3$NH$_3$PbBr$_3$ single crystal and shows a maximum external quantum efficiency of 3.17%, also higher than the reported 0.2% of the CH$_3$NH$_3$PbBr$_3$ single crystal. Our work may lead to more efficient self-powered heterojunction systems based on perovskite single crystals. *Published by AIP Publishing.* [http://dx.doi.org/10.1063/1.4971772]

Recent years have seen a quick boom of inorganic-organic lead halide perovskite materials due to their outstanding optoelectronic performances,[1] such as high light absorptivity and long-range balanced electronic- and hole-transport lengths, which are essential for an ideal solar cell.[2] However, perovskite materials prepared through solution methods often exist in the form of polycrystalline or amorphous films with a lot of boundaries, grains, and defects, resulting in the decrease of photovoltaic performance to a great extent.[3–5] Recently, organolead trihalide perovskite single crystals with low trap-state densities on the order of 10^9–10^{10} per cubic centimeter and long carrier diffusion exceeding 10 μm were reported. Also, the as-prepared perovskite single crystals exhibit a narrower band gap than the corresponding films, which means improved photocurrent generation and broader light absorption, suggesting their huge potential for photodetector applications.[6] So far, many attempts have been made to grow large-sized perovskite single crystals up to centimeters.[6–10] Thanks to the outstanding optoelectronic properties of perovskite single crystals compared to their corresponding polycrystalline film, a group of high-performance photodetectors based on perovskite single crystals have been exploited in recent years. Saidaminov and co-workers produced a planar-integrated single-crystalline MAPbBr$_3$ (CH$_3$NH$_3$ = MA) photodetector with a large responsivity exceeding 4000 A W^{-1} at the bias voltage of 5 V using a green monochromatic (λ = 520 nm) source.[11] Maculan and co-workers fabricated a MAPbCl$_3$ single crystal based photodetector with the responsivity of 46.9 mA W^{-1} at the bias voltage of 15 V under illumination with 365 nm UV light.[12] However, as we all know, the common operation modes of photodetectors based on the photovoltaic effect can be roughly divided into photoconduction and photocurrent,[13] for one-component single-crystal perovskite photodetectors based on the photoconduction mode, a certain operating voltage is

indispensable, which makes the photodetectors uneconomical. Therefore, self-powered photodetectors based on junctions, in which photo-generated carriers can be converted into current without external applied bias, are getting more and more attention. For example, Li and co-workers reported a TiO$_2$/MAPbI$_3$/HTM photodetector with a responsivity of 284 mA W^{-1} at 490 nm and 0 V bias.[14] Yu and co-workers demonstrated a broadband photodetector based on a ZnO/CH$_3$NH$_3$PbI$_3$ heterojunction and a MoO$_3$ hole-transport layer, showing a high photo-responsivity of 24.3 A W^{-1} at 500 nm without external bias voltage.[15] Fang and co-workers also attained a self-powered module by configuring a triboelectric nanogenerator (TENG) to the CH$_3$NH$_3$PbI$_3$ single crystal photodetector.[16] Nevertheless, so far, there is little work focusing on the preparation of single-crystalline perovskite heterojunction based photodetectors. In this article, we have developed a facile two-step approach to fabricate a perovskite heterojunction, which contains a single-crystalline MAPbBr$_3$ core and a crystalline MAPbI$_x$Br$_{3-x}$ shell with sharp frontier and interface between each pure component. The obtained MAPbBr$_3$ core shows high crystallinity and gives a bandgap of 2.16 eV, which is slightly lower than the reported 2.24 eV,[8] indicating a broader light absorption. The resulting MAPbBr$_3$/MAPbI$_x$Br$_{3-x}$ heterojunction with a specific core-shell structure exhibits higher photoresponsivity under the incident light with wavelengths of 350–800 nm than pure MAPbBr$_3$, and it achieves the highest photoresponsivity of 11.5 mA W^{-1} under 450 nm irradiation at 0 V bias.

The MAPbBr$_3$ single crystal with the size of 2 mm × 2 mm × 1 mm was prepared by inverse temperature crystallization, as previously reported.[8–10] For more details, see the supplementary material. We obtained the oversaturated mother liquor by heating the MAPbI$_3$/GBA solution on a hot plate maintained at 100 °C until small crystals appear. The MAPbBr$_3$ single crystal was vertically dipped into the oversaturated MAPbI$_3$/GBA solution for 2 s using a tweezer and then dried in the atmosphere of nitrogen. The crystal was

---
[a)]M. Cao and J. Tian contributed equally to this work.
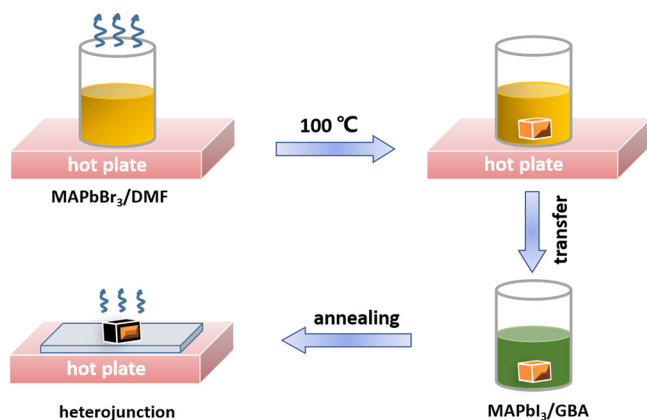[b)]Electronic mail: weidc@fudan.edu.cn

FIG. 1. Preparation process of the MAPbBr$_3$/MAPbI$_x$Br$_{3-x}$ heterojunction.

annealed at 100 °C for 5–10 min until it was completely dry, and the core-shell MAPbBr$_3$/MAPbI$_x$Br$_{3-x}$ heterojunction was obtained. The preparation process is illustrated in Fig. 1. Next, 10 μl of the as-prepared oversaturated MAPbI$_3$/GBA solution was spin-coated on the fluorine-doped tin oxide (FTO)-coated glass substrate at 2000 rpm for 10 s, and then, the heterojunction was put in the middle of the substrate and spin-coated at 3000 rpm. The whole device was annealed on a hot plate at 100 °C for 5 min to ensure a close contact between the perovskite heterojunction and the FTO substrate. The top black shell of the heterojunction was scraped off to expose the red core part; detailed photos are shown in Fig. S2 (supplementary material). Finally, a 50 nm thick Au electrode was deposited on the exposed MAPbBr$_3$ by thermal evaporation with a mask of 0.004 cm^2, and then, two wires were connected onto the surface using moderate silver conductive paste.

To confirm the morphology and the formation of the perovskite heterojunction, we conducted two combined characterization methods including Field-emission scanning electron microscopy-Energy dispersive X-ray spectroscopy (FESEM-EDS, Zeiss Ultra 55) and Powder X-ray diffraction (XRD, PANalytical X'pert PRO) of two separated layers in

the heterojunction, as shown in Fig. 2. FESEM images of the section obtained by cutting the heterojunction just in the middle are shown in Fig. 2(a), top view and in Figure 2(b), side view. An obvious boundary of bromide and iodide can be seen in Fig. 2(c), implying that the single-crystalline MAPbBr$_3$ core is encased in a crystalline MAPbI$_x$Br$_{3-x}$ shell with a thickness of about 7 μm. To identify the chemical composition, EDS analysis was carried out on the heterojunction. Figs. 2(d)–2(f) display the element mapping results, indicating that the element of the shell region is mainly iodide, incorporated with C, N, Pb, and some bromide, whereas its core counterpart is bromide dominated. Further evidence comes from the XRD spectra of both the core and the shell part in Fig. 2(g). The powder XRD of the shell part shows diffraction peaks at 14.95°, 29.97°, and 33.59° corresponding to the (100), (200), and (210) lattice planes, with the full width of half maximum (FWHM) from 0.1° to 0.3°. Moreover, it is obvious that the diffraction peaks shift to a lower angle compared to pure MAPbBr$_3$, indicating an increased lattice constant after introducing I with a larger atomic size, which is consistent with the results reported before.[17] As for the core part, the powder XRD shows diffraction peaks at 15.36°, 30.52°, and 34.18°, which correspond to (100), (200), and (210) lattice planes as well and its FWHM is about 0.1°. This result is consistent with the powder XRD of the MAPbBr$_3$ single crystal and the reported sample.[8] Therefore, we safely conclude that the core part, with better stability and crystallinity, is still the MAPbBr$_3$ single crystal, while it is covered by MAPbBr$_x$I$_{3-x}$ (x < 3) outside. A typical energy dispersive spectroscopy (EDS) spectrum of the crystalline MAPbI$_x$Br$_{3-x}$ shell is shown in Fig. S3 (supplementary material), and x is calculated to be 1.76 (the atomic ratio of Br/I is calculated to be 0.71) according to the quantitative analysis. Moreover, after being stored for one month, the heterojunction remained stable with unchanged shell composition, as shown in Fig. S4 (supplementary material).

Studies of current–voltage (I–V) characteristics of the core-shell perovskite reveal the presence of a good heterojunction
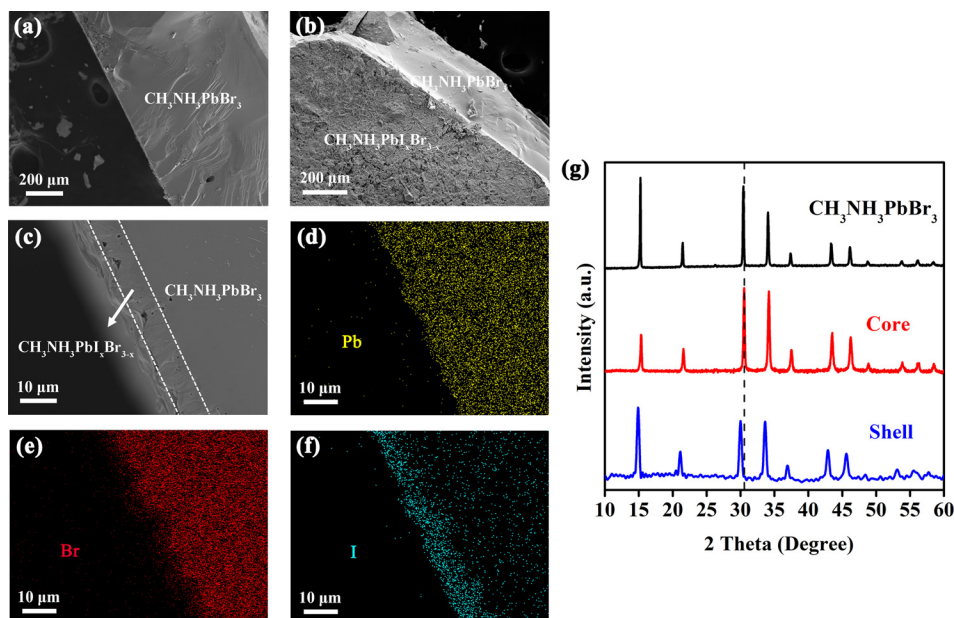

FIG. 2. Characterization of the MAPbBr$_3$/MAPbI$_x$Br$_{3-x}$ heterojunction. (a) Top view and (b) side view FESEM images of a section of the MAPbBr$_3$/MAPbI$_x$Br$_{3-x}$ heterojunction. (c) A magnified view of image (a). (d)–(f) Element mapping images of Br, I, and Pb for the section shown in (c). (g) X-ray diffraction patterns of the ground powder from the MAPbBr$_3$ single crystal, core part, and shell part.

between MAPbBr$_3$ and MAPbI$_x$Br$_{3-x}$. Fig. 3(a) shows the I–V characteristic of the MAPbBr$_3$/MAPbI$_x$Br$_{3-x}$ heterojunction based on symmetrical silver electrodes. The device exhibited an obvious increase in current as well as a better rectifying diode-like behavior with a small leakage current to be 10^{-7} A and a forward current to be 10^{-6} A at 10 V bias under 450 nm irradiation. To investigate the performance of this heterojunction, we employed a device to test its photoresponse. A schematic device structure of the photodetector based on the MAPbBr$_3$/MAPbI$_x$Br$_{3-x}$ heterojunction is illustrated in the inset of Fig. 3(b). The heterojunction was constructed on the FTO-glass substrate with a 50 nm gold film as the anode. According to the current–density–voltage curve given in Fig. 3(b), the device also showed a photovoltaic behavior with a short-circuit photocurrent of 0.1961 mA cm^{-2}, an open-circuit voltage of 0.61 V, and a fill factor of 0.413. The current–density–voltage (J-V) curve was measured under simulated AM 1.5 G illumination provided by a 500 W xenon lamp (So1ar-500, NBeT).

We further studied the wavelength-dependent photoresponse of the photodetector under the incident light with wavelengths of 350–800 nm and the photoresponsivity at zero bias is summarized in Fig. 3(d). The photoresponsivity (R) is calculated according to the formula, R = (I$_{light}$−I$_{dark}$)/P$_{light}$, where I$_{light}$ and I$_{dark}$ are the photocurrent and dark current, respectively, obtained by measuring the current–voltage

(I–V) characteristics under the dark condition and different incident wavelengths, respectively, and P$_{light}$ is the power of the incident light. Unlike the highly narrowband perovskite single-crystal photodetectors,[17] our device showed a broad photoresponse ranging from 350 to 800 nm and achieved a peak responsivity up to 11.5 mA W^{-1} under 450 nm irradiation. The maximum responsivity we obtained is similar to the photodetector based on n-i-p TiO$_2$/spin-coated MAPbI$_3$/spiro-OMeTAD semiconductor junctions with careful interface engineering, which achieves a peak responsivity as high as 0.395 A W^{-1} at 600 nm wavelength,[18] and the maximum external quantum efficiency (EQE) obtained was 3.17% (Fig. S5 of the supplementary material), also higher than the reported 0.2% of MAPbBr$_3$ single crystal with a thickness of 1.2 mm.[17] Compared with the broadband photodetector based on a ZnO/CH$_3$NH$_3$PbI$_3$ heterojunction and a MoO$_3$ hole-transport layer, which was also fabricated on a FTO-glass with an Au electrode as the top electrode and showed a photo-responsivity of 24.3 A W^{-1},[15] the responsivity of our device is relatively low, indicating that it is possible to improve the performance of the photodetector by introducing a hole-transport layer. Finally, the temporal photoresponse of the MAPbBr$_3$/MAPbI$_x$Br$_{3-x}$ photodetector was measured under 5 μW illumination at 450 nm and zero bias; the corresponding photo-switching characteristics are shown in Fig. 3(e). The photodetector exhibited good on–off switching
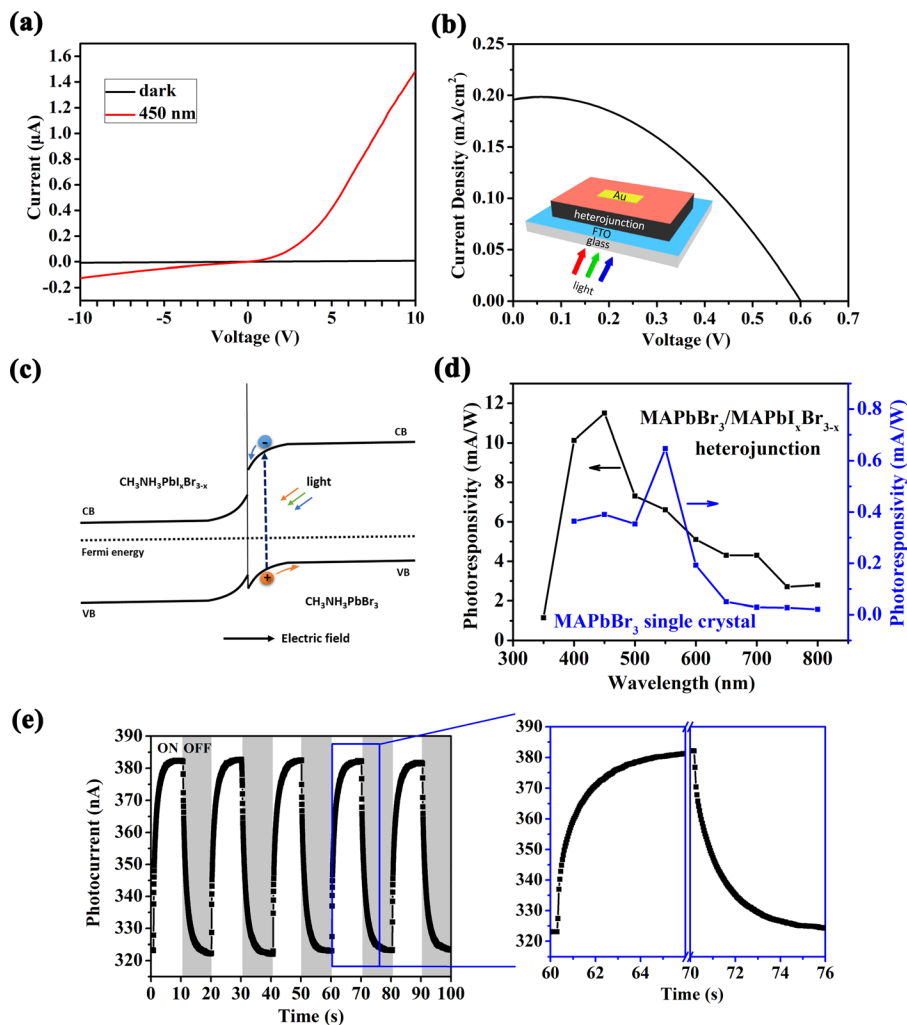

FIG. 3. Device architecture and performance. (a) Current–voltage characteristics of the core-shell perovskite heterojunction based on the symmetrical silver electrodes under 450 nm irradiation (red) and in the dark (black). (b) J–V characteristics under a xenon lamp (inset image is the schematic diagram of the photodetector). (c) Schematic energy level diagram at the MAPbBr$_3$/MAPbI$_x$Br$_{3-x}$ junction under irradiation. (d) Responsivity of MAPbBr$_3$/MAPbI$_x$Br$_{3-x}$ and single-crystal MAPbBr$_3$ photodetectors at zero bias under the incident light with wavelengths of 350–800 nm and 400–800 nm, respectively. (e) Photo-switching characteristics of the MAPbBr$_3$/MAPbI$_x$Br$_{3-x}$ photodetector under alternating dark and light illumination (5 μW, 450 nm) at zero bias. The right panel shows an enlarged view of the temporal photocurrent response during on–off illumination switching.

with a rise time of 2.3 s and a fall time of 2.76 s. The ON–OFF switching behavior was reserved over multiple cycles, indicating the stability of our photodetector. We also built a MAPbBr$_3$ single crystal based photodetector, which was fabricated and measured under the same conditions, to make a contrast with the heterojunction. Compared to the photoresponse of the MAPbBr$_3$ single crystal photodetector shown in Fig. 3(d), the responsivity of the heterojunction was increased by one order of magnitude. The fabricated MAPbBr$_3$ photodetector also showed a broadband spectral response upon bottom illumination, since photogenerated charge carriers can be collected efficiently in the vicinity of the electrodes, in accordance with previous reports.[11,19] Moreover, the MAPbBr$_3$ based photodetector exhibited the peak EQE of 0.14% at 550 nm (Fig. S5 of the supplementary material), which is close to the reported 0.2%,[17] confirming the enhanced performance of our core-shell heterojunction. The improved performance is a result of exciton dissociation with the help of the built-in electric field in the heterojunction. Photo-generated electron-hole pairs are separated by a strong local electric field arising from the band bending at the junction, the electrons are injected into MAPbI$_x$Br$_{3-x}$, and the holes are transferred to MAPbBr$_3$, leading to a remarkable photocurrent at zero bias. The corresponding energy level diagram is presented in Fig. 3(c). As seen from the diagram, electron injection from MAPbBr$_3$ to MAPbI$_x$Br$_{3-x}$ is more likely than hole injection from MAPbI$_x$Br$_{3-x}$ to MAPbBr$_3$ considering the hole barrier in the valence band, resulting in a spatial separation of electrons and holes; thus, the charge recombination was suppressed. This, as well as the increased photoconductivity of the shell under irradiation, leads to a remarkable photoresponsivity of the heterojunction. Meanwhile, the photo-generated electron-hole pairs in single MAPbBr$_3$ are easy to recombine without the external electric field provided by the applied bias. The responsivity of photodetectors was measured using a 300 W xenon lamp (HSX-UV300, PE) with a monochromator (NBeT). A semiconductor device analyzer (Keysight, B1500A) with a probe station was used for the photocurrent measurement. Monochromatic light with wavelengths between 350 nm and 800 nm was applied to the samples through an optical fiber.

In summary, we have developed a facile two-step approach to fabricate a core-shell perovskite heterojunction based on the CH$_3$NH$_3$PbBr$_3$ single crystal. Characterization such as FESEM-EDS and XRD confirms the formation of heterojunction. The photodetector based on the heterojunction showed a typical photovoltaic behavior as well as a wavelength-dependent responsivity with a peak responsivity up to 11.5 mA W^{-1} under 450 nm irradiation at zero bias, which is about one order of magnitude higher than the CH$_3$NH$_3$PbBr$_3$ single crystal photodetector and exhibited a maximum external quantum efficiency of 3.17%, also higher than the reported 0.2% of CH$_3$NH$_3$PbBr$_3$ single crystal with a thickness of 1.2 mm. Our work may lead to a more efficient self-powered heterojunction system based on perovskite single crystals.

See supplementary material for the experimental details on synthesis of perovskite, XRD characterization and quantitative analysis of the heterojunction, and external quantum efficiency of the single-crystal MAPbBr$_3$ photodetector under 400–800 nm irradiation at zero bias.

[1]S. D. Stranks and H. J. Snaith, Nat. Nanotechnol. **10**, 391 (2015).
[2]G. Xing, N. Mathews, S. Sun, S. S. Lim, Y. M. Lam, M. Grätzel, S. Mhaisalkar, and T. C. Sum, Science **342**, 344 (2013).
[3]A. Kojima, K. Teshima, Y. Shirai, and T. Miyasaka, J. Am. Chem. Soc. **131**, 6050 (2009).
[4]K. Wang, C. Liu, P. Du, H. L. Zhang, and X. Gong, Small **11**, 3369 (2015).
[5]N. J. Jeon, J. H. Noh, W. S. Yang, Y. C. Kim, S. Ryu, J. Seo, and S. I. Seok, Nature **517**, 476 (2015).
[6]D. Shi, V. Adinolfi, R. Comin, M. Yuan, E. Alarousu, A. Buin, Y. Chen, S. Hoogland, A. Rothenberger, K. Katsiev, Y. Losovyj, X. Zhang, P. A. Dowben, O. F. Mohammed, E. H. Sargent, and O. M. Bakr, Science **347**, 519 (2015).
[7]Q. Dong, Y. Fang, Y. Shao, P. Mulligan, J. Qiu, L. Cao, and J. Huang, Science **347**, 967 (2015).
[8]Y. Liu, Z. Yang, D. Cui, X. Ren, J. Sun, X. Liu, J. Zhang, Q. Wei, H. Fan, F. Yu, X. Zhang, C. Zhao, and S. F. Liu, Adv. Mater. **27**, 5176 (2015).
[9]J. M. Kadro, K. Nonomura, D. Gachet, M. Grätzel, and A. Hagfeldt, Sci. Rep. **5**, 11654 (2015).
[10]M. I. Saidaminov, A. L. Abdelhady, B. Murali, E. Alarousu, V. M. Burlakov, W. Peng, I. Dursun, L. Wang, Y. He, G. Maculan, A. Goriely, T. Wu, O. F. Mohammed, and O. M. Bakr, Nat. Commun. **6**, 7586 (2015).
[11]M. I. Saidaminov, V. Adinolfi, R. Comin, A. L. Abdelhady, W. Peng, I. Dursun, M. Yuan, S. Hoogland, E. H. Sargent, and O. M. Bakr, Nat. Commun. **6**, 8724 (2015).
[12]G. Maculan, A. D. Sheikh, A. L. Abdelhady, M. I. Saidaminov, M. A. Haque, B. Murali, E. Alarousu, O. F. Mohammed, T. Wu, and O. M. Bakr, J. Phys. Chem. Lett. **6**, 3781 (2015).
[13]K. F. Mak and J. Shan, Nat. Photon. **10**, 216 (2016).
[14]D. Li, G. Dong, W. Li, and L. Wang, Sci. Rep. **5**, 7902 (2015).
[15]J. Yu, X. Chen, Y. Wang, H. Zhou, M. Xue, Y. Xu, Z. Li, C. Ye, J. Zhang, P. A. van Aken, P. D. Lund, and H. Wang, J. Mater. Chem. C **4**, 7302 (2016).
[16]H. Fang, Q. Li, J. Ding, N. Li, H. Tian, L. Zhang, T. Ren, J. Dai, L. Wang, and Q. Yan, J. Mater. Chem. C **4**, 630 (2016).
[17]Y. Fang, Q. Dong, Y. Shao, Y. Yuan, and J. Huang, Nat. Photonics **9**, 679 (2015).
[18]B. R. Sutherland, A. K. Johnston, A. H. Ip, J. Xu, V. Adinolfi, P. Kanjanaboos, and E. H. Sargent, ACS Photonics **2**, 1117 (2015).
[19]M. I. Saidaminov, M. A. Haque, M. Savoie, A. L. Abdelhady, N. Cho, I. Dursun, U. Buttner, E. Alarousu, T. Wu, and O. M. Bakr, Adv. Mater. **28**, 8144 (2016).